ELSEVIER

International Journal of Adhesion & Adhesives 28 (2008) 302–313

International Journal of Adhesion & Adhesives

www.elsevier.com/locate/ijadhadh

Continuum damage modelling of environmental degradation in joints bonded with EA9321 epoxy adhesive

Y. Hua[a], A.D. Crocombe[a,*], M.A. Wahab[a], I.A. Ashcroft[b]

[a]*School of Engineering (H5), University of Surrey, Guildford GU2 7XH, UK*
[b]*Wolfson School of Mechanical and Manufacturing Engineering, Loughborough University, Loughborough LE11 3TU, UK*

Accepted 20 August 2007
Available online 7 November 2007

Abstract

A mesh-independent continuum damage model has been proposed to predict the residual strength of adhesively bonded joints by introducing a displacement-based damage parameter into the constitutive equation of damaged materials. Joints bonded with a ductile adhesive EA9321 were studied for a range of environmental degradation. The moisture-dependent damage parameter for EA9321 was calibrated using an aged, mixed-mode flexure (MMF) test. The parameter was then used without further modification to model failure in aluminium and composite single-lap joints (SLJ) bonded with the same adhesive. The finite element analysis (FEA) package ABAQUS was used to implement the coupled mechanical-diffusion analyses required. The elastic–plastic response of the adhesive and the substrates, both obtained from the bulk tensile tests, were incorporated. A von Mises yield model was considered and both 2D and 3D modelling were undertaken and the results compared. The predicted joint residual strengths agreed well with the corresponding experimental data and the damage propagation pattern in the adhesive was also predicted correctly. The mesh independence of the model was demonstrated. This continuum damage model provides a means of predicting environmental degradation in ductile adhesive-bonded joints, where failure is predominantly within the adhesive layer.

Keywords: B. Aluminium and alloys; C. Finite element stress analysis; D. Durability; Progressive damage modelling

1. Introduction

The advantages of adhesive bonding over traditional joining techniques have been well accepted. Compared with other joining techniques, adhesive bonding can distribute load over a much wider area, reduce stress concentrations, increase fatigue and corrosion resistance of the bonded joints, and provide weight savings to the whole structure and the ability to join different materials. They have been used in automotive, aerospace and electronic packaging industries. However, the lifetime of bonded joints are difficult to model accurately and their long-term performance cannot easily and reliably be predicted, especially under the combined effects of an aggressive environment and mechanical loading. This has been one of the main restrictions to a more widespread use of adhesives.

A commonly encountered hostile environment is exposure to moisture, often at elevated temperatures. The problem of durability of adhesive joints to hostile environments has become the main challenge for researchers in this area. Many kinds of experimental techniques have been undertaken to deal with this problem. It has been found that the degradation of the bonded joint depends on the type of substrate and adhesive, the type of surface pretreatment, the loading configuration and the ageing environment [1]. Two main types of failure, interfacial and cohesive, are commonly found for adhesive joints: failure sites are at the adhesive/substrate interface, or cohesive within the adhesive, respectively.

Predictive modelling can help reduce the uncertainty in the residual strength after prolonged service. Finite element analysis (FEA) has been employed to develop durability prediction models based on progressive failure analysis [2–5]. This work has focused on material separation modelling using a predefined crack propagation path and

*Corresponding author. Tel.: +44 1483 689 194; fax: +44 1483 306 039.
E-mail address: a.crocombe@surrey.ac.uk (A.D. Crocombe).

0143-7496/$ - see front matter © 2007 Elsevier Ltd. All rights reserved.
doi:10.1016/j.ijadhadh.2007.08.005

an interfacial rupture element. Such an approach is generally known as cohesive zone modelling (CZM). Recently, a strain-based continuum failure model has been proposed by the authors [6] to deal with progressive cohesive failure in ductile adhesive-bonded joints, and considerable success has been achieved. However, the mesh dependence that results with a strain-based failure parameter is a big disadvantage to this approach. To overcome this problem, a displacement-based continuum damage model has been proposed and demonstrated in this paper. It has shown a higher potential to predict cohesive failure in ductile adhesive-bonded joints.

2. Background

A detailed background of the approaches recently developed to deal with general progressive ductile material failure has been reviewed by the authors elsewhere [6,7]. Only a very brief summary is presented here. Four approaches have attracted most of the attention in this area. They are the virtual internal bond (VIB) model, the porosity-based Gurson model, the continuum damage mechanics (CDM) model and the simple, strain-based cohesive failure model.

The VIB model [8,9] represents the continuum as a random network of discretely connected material points which can incorporate plasticity [10–12]. However, such an approach is more suited to modelling material at the micro- rather than the macroscopic level and tends to exhibit size dependency, for reasons outlined elsewhere [6,7]. The Gurson model [13] is based on the growth of a void in an elasto-plastc continuum. Efforts have been made to extend this approach to spread the damage process [14–18]. However in any of these forms a large number of material parameters are required resulting in a significant number of characterizing tests [19,20] and these parameters can experience size and mesh effects. Unlike the mechanistically based Gurson model, the CDM approach [21,22] is phenomenological in nature. Damage is introduced as a state variable that affects the macroscopic constitutive response and such an approach usually results in far fewer material parameters than the Gurson approach. As with the Gurson approach it can experience size and geometry effects [23].

Recently, a strain-based cohesive failure model has been proposed [6] to predict progressive damage failure in ductile adhesive-bonded joints. This is the simplest method of modelling progressive continuum failure within FE analysis. Material followed the non-linear constitutive response until the maximum equivalent plastic strain reached a critical value at any element integration point. This critical strain was obtained from mixed-mode flexure (MMF) calibration tests at different levels of moisture concentration. An element with all the nodes in excess of this critical strain failed. The failed elements formed a natural failure propagation path in the model. This model has been used successfully in predicting the damage initiation and propagation as well as the failure loads in a range of environmentally degraded joints bonded with the ductile adhesive EA9321. One problem with this method is the mesh dependence, observed when analysing configurations with singular-stress fields. This can restrict its use as a general continuum damage modelling method.

In this paper, a mesh-independent continuum damage model is presented and used to undertake progressive damage modelling of joint systems bonded with EA9321. A damage parameter is introduced into the constitutive equation of damaged materials, which is defined in form of the displacement of elements rather than the strain. Damage in an element starts once this parameter is greater than zero, and when it reaches its maximum value of 1, the element fails. This is discussed in more detail in the next section. The failed elements form a fully damaged path in the model, which is similar to the strain-based failure model. Thus, this continuum damage model predicts not only the failure loads of the joints but also the damage initiation and propagation in the adhesive. The moisture-dependent damage parameters of EA9321 have been obtained from MMF calibration tests at different levels of moisture concentration. A coupled diffusion-mechanical analysis was undertaken using the commercial finite element package ABAQUS. The moisture uptake behaviour of the adhesive during ageing was characterised based on Fick's law [24], which has been widely used in modelling the diffusion in adhesively bonded structures. It is possible that much of this damage is reversible as the exposed joints dry, but this is an aspect that has not yet been fully investigated.

2.1. Overview of the mesh-independent continuum damage model

The essential concept of the continuum damage failure model is to introduce a damage parameter, D, to represent the effect of damage in the constitutive equation of the material. This is achieved by reducing the stress of the undamaged material in proportion to the damage parameter as shown in Eq. (1). The resulting degradation

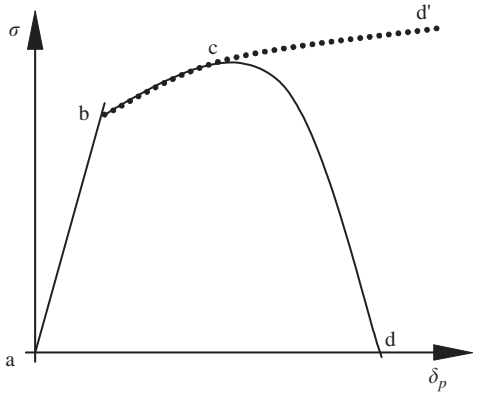

Fig. 1. A damaged material response based on the equivalent plastic displacement using the continuum damage failure model.

process is schematically shown in Fig. 1. The material response is initially linear (a–b), followed by plastic irreversible yielding with strain hardening (b–c). Point c identifies the material state at the onset of damage, which is defined using a damage initiation criterion. Beyond this point, the stress–strain response (c–d) is governed by a specified damage evolution law as shown in Eq. (1). At point d, the material has lost its load-carrying capacity, corresponding to the fully damage state ($D = 1$). In the context of damage mechanics c–d can be viewed as the degraded response of the curve c–d′ that the material would have followed in the absence of damage.

$$\sigma_d = (1 - D)\sigma, \quad D = f(\delta_p), \quad 0 \leqslant D \leqslant 1. \tag{1}$$

This damage parameter, D, is specified in terms of the equivalent plastic displacement, δ_p, rather than strain, ε_p, to ensure no mesh dependency in the modelling. This is as shown in Eq. (1). With this approach, the softening response after damage initiation is characterised by a stress–displacement response rather than a stress–strain response. The implementation of this stress–displacement concept in a finite element model requires the definition of a characteristic length, L, associated with an integration point. The energy to rupture is then given in Eq. (2) in terms of the equivalent stress σ_p and the equivalent plastic displacement δ_p

$$G_f = \int_{\varepsilon_{p,0}}^{\varepsilon_{p,f}} L\sigma_p \dot{\varepsilon}_p = \int_0^{\delta_{p,f}} \sigma_p \dot{\delta}_p. \tag{2}$$

This expression introduces the definition of the equivalent plastic displacement, δ_p, as the fracture work conjugate of the yield stress after the onset of damage (work per unit area of the crack) as shown in Eq. (3):

$$\begin{aligned} &\delta_p = 0, \quad \text{before damage initiation,} \quad D = 0 \\ &\dot{\delta}_p = L\dot{\varepsilon}_p, \quad \text{after damage initiation,} \quad 0 < D1. \end{aligned} \tag{3}$$

This method is available within ABAQUS [25]. The moisture-dependent damage parameter (D), which defines the damage curve c–d as shown in Fig. 1, requires calibration before use in predictive modelling.. The data input to ABAQUS is the damage-equivalent plastic displacement curve. This calibration process is discussed further in the later modelling sections of this paper.

To determine the actual behaviour of elements in a model the equivalent plastic displacement is obtained from the equivalent plastic strain (an element parameter) using a characteristic length, L, calculated in terms of the element size. The value of this characteristic length is based on the element geometry. For shell and planar elements the square root of the integration point area is used. For solid elements the cube root of the integration point volume is used. This definition of the characteristic length is used because the direction in which fracture occurs is not known in advance. Therefore, elements with large aspect ratios will have rather different behaviour depending on the direction in which they crack. Some mesh sensitivity may remain because of this effect, and elements that have aspect ratios close to unity are recommended. This is discussed in more detail later.

3. Experimental methodology and materials characterisation

Only a summary of the key data is presented here. More information can be found in an earlier paper [6]. The adhesive under investigation is a two-part epoxy paste adhesive Hysol EA9321 (Henkel Aerospace, Bay Point, CA, USA). This has been used to produce cured bulk adhesive sheets (0.5 mm thick), MMF joints with aluminium 7075-T6 substrates and standard single-lap joints (SLJ) with 3-mm-thick aluminium (7075-T6) substrates or 2-mm-thick composite (IM7-8552) substrates. The composite substrates were lightly abraded and solvent wiped whilst the aluminium substrates were subjected to a chromic acid etch. Further manufacturing details are given elsewhere [6].

The bulk adhesive films were machined into dumbell specimens, which were first used to determine diffusion parameters using gravimetric moisture uptake tests in a 50 °C and 95.8% RH environment. It was found that the uptake response fitted the Fickian model given in Eq. (4). The diffusion coefficient (D) and the equilibrium mass uptake (m_∞) are listed in Table 1. More experimental details are presented in [6]

$$\frac{m_t}{m_\infty} = 1 - \frac{8}{\pi^2}\sum_{n=0}^{\infty}\frac{1}{(2n+1)^2}\exp\left[\frac{-D(2n+1)^2\pi^2 t}{4l^2}\right]. \tag{4}$$

Both wet and dry bulk specimens were tested in uniaxial tension and the resulting data can be seen in Fig. 2. In the FE modelling the material behaviour of EA9321 at intermediate moisture levels was determined by linear interpolation between results from the dry and the saturated conditions.

The MMF configuration, shown in Fig. 3, was used to calibrate the moisture-dependent critical strain parameter of the adhesive. It is a significantly different configuration to the SLJ specimens tested later and hence a good test of the general applicability of the cohesive failure model. The adhesive was cured on the upper substrate and this was exposed in an open-faced condition (to achieve quick and uniform degradation in the adhesive layer) in different environments before a secondary bond was used to attach the lower substrate and complete the specimen. A 20 mm pre-crack was introduced on the EA9321

Table 1
Fickian diffusion data for 0.48-mm-thick EA9321

Ageing environment	95.8% RH, 50 °C
Diffusion coefficient (m^2/s)	3.0×10^{-13}
Equilibrium mass uptake (m_∞)	3.85%

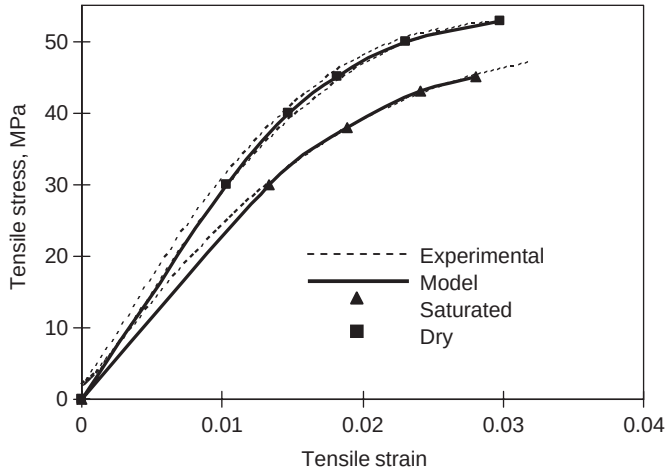

Fig. 2. Moisture-dependent tensile properties of bulk EA9321.

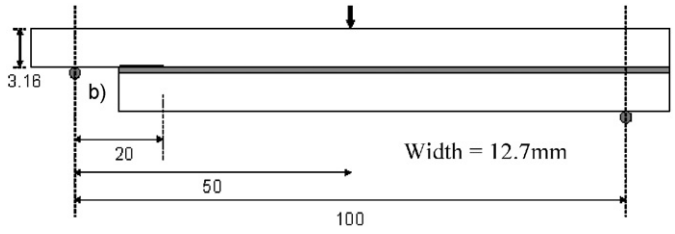

Fig. 3. Geometry and loading configuration of the MMF specimen.

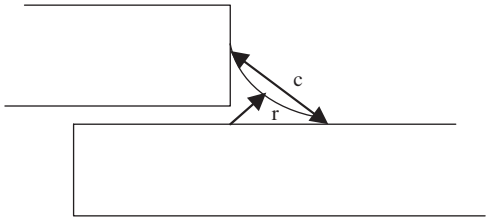

Fig. 4. Fillet configuration of the EA9321-bonded SLJs (not to scale).

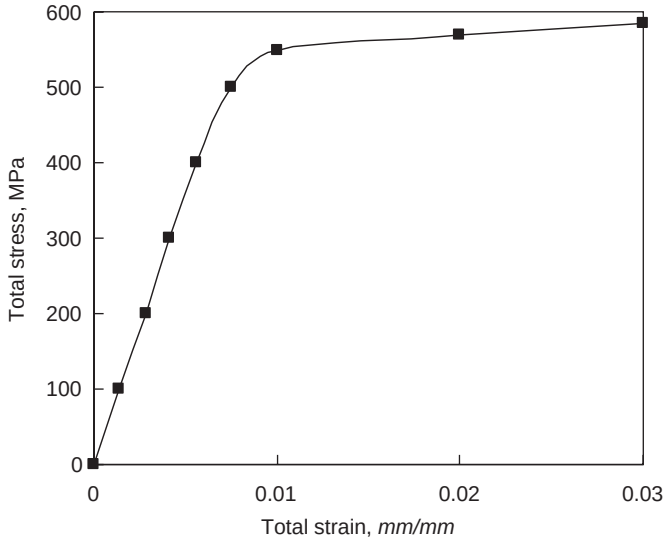

Fig. 5. Tensile properties of aluminium substrates ($E = 72$ GPa, $v = 0.3$) [26].

Table 2
IM7-8552 Properties used for modelling [27]

E_{11} (GPa)	E_{22} (GPa)	E_{33} (GPa)	G_{12} (GPa)	G_{13} (GPa)	G_{32} (GPa)	v_{12}	v_{13}	v_{32}
160	10	10	4.8	4.8	3.2	0.31	0.31	0.52

Table 3
Fickian diffusion data for IM7-8552 unidirectional CFRP [6]

Moisture environment	D-parallel to fibre axis (m^2/s)	D-perpendicular to fibre axis (m^2/s)	Equilibrium mass uptake (%mwt$_\infty$)
95.8% RH, 50 °C	7×10^{-13}	2×10^{-13}	~1.0

adhesive–aluminium interface using a teflon film. The fracture loads recorded for the MMF tests were used in conjunction with the FEA modelling to determine the moisture-dependent critical strain of the adhesive. More experimental details can be found elsewhere [6].

The fillet size in the SLJs was about 0.62 mm/0.90 mm by radius(r)/chord(c) as illustrated in Fig. 4. The material properties of 7075-T6 and IM7-8552 [26,27], are shown in Fig. 5 and Table 2, respectively. The Fickian diffusion parameters of the composite are shown in Table 3 [6]. The joints were aged at 50 °C, 95.8% RH for various periods of time before being withdrawn for testing. At each withdrawal time there were five replicate aluminium and three replicate composite SLJs. It was found that the failure of the EA9321/aluminium joints were all primarily cohesive in the adhesive near to the interface and the failure of the EA9321/composite joints were a combination of cohesive failure in the adhesive close to interface and delamination of the substrate. These experimental results were used to validate the prediction of the cohesive failure model using FEA modelling.

4. 2D progressive damage modelling

The moisture-dependent damage parameter (D) was calibrated by matching the predicted and experimental MMF test results. The moisture-dependent undamaged material response was based on the experimental material curves of the adhesive shown in Fig. 2. A range of damage initiation and damage failure points were considered and their effect on the predicted MMF response was studied. A 2D FE model with mesh refinement of 0.1 mm × 0.1 mm along the adhesive layer is shown in Fig. 6. It has been noted that to ensure mesh independency of the modelling, elements that have aspect ratios close to unity are recommended.

Plane strain four-noded quadrilateral elements were used. The continuum damage model is only available for

explicit analysis in ABAQUS. Von Mises yielding was assumed for the adhesive. A mass scaling factor of 1×10^5 was used to prevent dynamic instability. This value provided a time efficient solution that did not significantly affect the accuracy of the static analyses. Nonlinear geometric behaviour was included in the modelling.

To simplify the calibration of the material softening curve of the continuum damage model, a damage initiation point (point c shown in Fig. 1) and a failure point (corresponding to the zero stress point d shown in Fig. 1) were chosen as the two failure determining parameters, which formed a straight softening line for the damaged EA9321. Then the "completed" material property was incorporated into the FE model and the predicted failure load was compared to the experimental result. To study the effect of the parameters on the predicted results, four selected calibration strain–stress curves for the dry condition were considered, as shown in Fig. 7(a). The corresponding predictions that were obtained are shown in Fig. 7(b).

It can be seen in Fig. 7 that an increase of the damage initiation or failure parameters both led to a higher failure load prediction. Further, curves which had similar areas (Calibrations 2 and 3 in Fig. 7(a)) gave similar predictions for the experimental failure load. A tentative conclusion can be drawn based on the above observations and other similar analyses, that the envelop area resulting from the enclosed stress–displacement curve dominates the continuum damage modelling, regardless of the damage initiation and propagation positions. Considering that the area represents the fracture energy, this is consistent with fracture mechanics. However, this does not mean that the softening curve can take any shape. In this work, Calibration 3, rather than Calibration 2, has been chosen because the damage occurs from the end point of the measured experimental data.

To make the calibrated softening curve more realistic it was decided to modify the simple straight line shown in Fig. 7(a) to provide more curvature, as shown in Fig. 8(a). Calibration of another moisture concentration level (the saturation condition at 95.8% RH/50 °C, $m_\infty = 3.85\%$, as illustrated in Table 1) was also undertaken. The selected calibration data are shown in Fig. 8(a). The predicted result of the MMF specimen at a normalised moisture

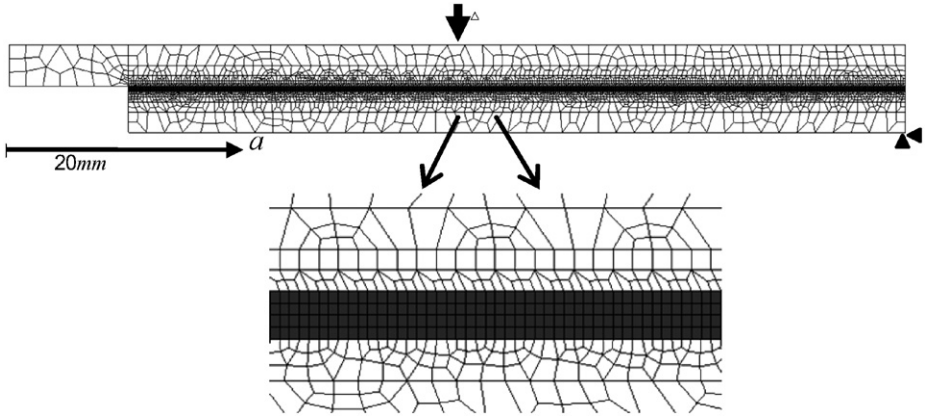

Fig. 6. MMF FE model with mesh refinement along the adhesive overlap.

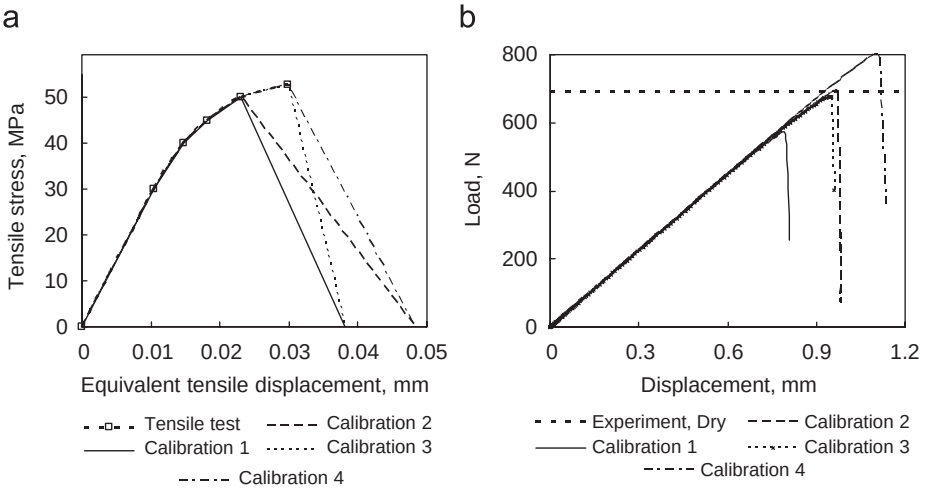

Fig. 7. The damage curve calibrations of dry EA9321 using the MMF model (smallest mesh size 0.1 mm × 0.1 mm): (a) calibration curves (of unit-size elements); (b) predicted loading history.

concentration level of 0.545 is shown in Fig. 8(b) along with the corresponding experimental data. A linear interpolation between the dry and saturated data has been assumed in the predictive modelling. Three different mesh refinement sizes were used and compared. The predicted failure loads demonstrated satisfactory mesh independence in the modelling, as shown in Fig. 8(b).

The MMF calibrated damage parameters for EA9321 were used without any modification to predict the response of the aluminium and composite SLJs using the continuum damage model.

(a) *EA9321/aluminiumSLJ model*: A 2D finite element model of the EA9321/aluminium SLJ is shown in Fig. 9, with a 0.05 mm × 0.05 mm mesh of plane strain four-noded quadrilateral elements along the adhesive layer. Due to the symmetry of the SLJ configuration, only half the joint was modelled. Rotational symmetry was applied to a section through the middle of the overlap. As with the MMF analysis, explicit analysis was used with a mass scaling factor of 1×10^5. Geometric nonlinearity was also taken into account.

Standard Fickian diffusion was used to obtain the moisture profiles along the overlap length. The mass diffusion model coded in ABAQUS [25] was used to generate the normalised nodal moisture concentration as field output for the coupled diffusion-mechanical analysis, using the diffusion parameters shown in Table 1. Results are similar to those reported elsewhere [6]. The same moisture-dependent damage curves calibrated from the MMF tests (shown in Fig. 8(a)) were used for the SLJ modelling. The variation of the residual strengths with time of exposure of the joints obtained from the experimental results and the finite element modelling are shown in Fig. 10. It can be seen that the FE modelling predictions with different mesh schemes agreed well with each other and with the experimental results. Relatively lower failure loads were predicted for the joints degraded for 2 and 4 weeks, compared to the average results obtained from the

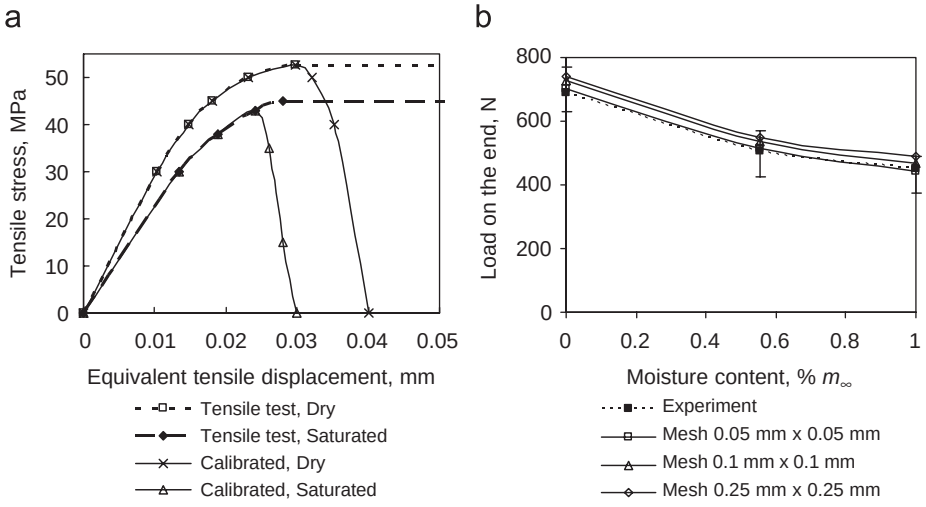

Fig. 8. The mesh-independent, moisture-dependent damage curves calibration: (a) calibrated results; (b) predicted failure loads of the MMF specimen.

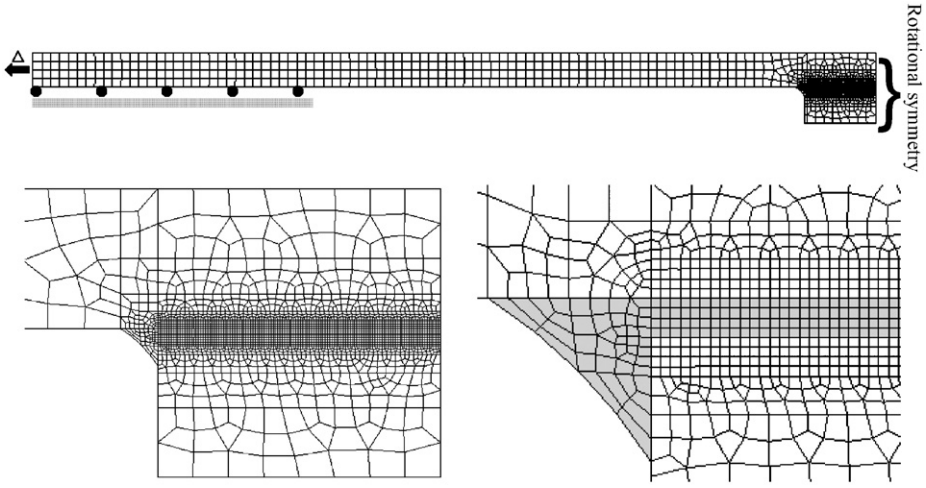

Fig. 9. FE model of the EA9321/aluminium SLJ and local mesh refinement.

experiments. This may be because the assumption of linear interpolation between the two calibrated damage curves is not entirely appropriate.

The damage initiation and propagation in the joint (within the adhesive layer) can also be predicted using the continuum damage model. A series of contour plots selected from the joint degraded for 26 weeks with the 0.05 mm × 0.05 mm mesh scheme are shown in Fig. 11. The damage parameter, SDEG (stiffness degradation) in ABAQUS, records the degree of damage ($D = 0$–1) in the elements. Thus non-coloured elements in Fig. 11 are undamaged. It can be seen that the damage initiated around the corner of the unloaded substrate (a), propagated across the adhesive layer, through the fillet and along the lower interface (b). The damage then built up and extended in the fillet and along the lower interface with no significant growth on the upper interface (c) and (d), finally extending completely to the middle of the joint (e). This is similar to the modelling results from the strain-based failure model [6]. However, in the strain-based model, only the completely failed elements can be identified to show the damage and thus cannot give a full contour map for the damage in the adhesive.

Curves showing the predicted loading history and damage propagation obtained from an undegraded joint and a joint degraded for 26 weeks with the 0.05 mm × 0.05 mm mesh are shown in Fig. 12. It was seen that the load in the undegraded specimen increased linearly with applied displacement and peaked at about 9.02 kN before suddenly failing. The damage in the adhesive initiated and propagated very quickly. The predicted loading history of the 26-week-degraded joint appeared to give a similar response. However there was a slight degree of non-linearity in the response. In this degraded model, the damage initiated at an applied displacement level of

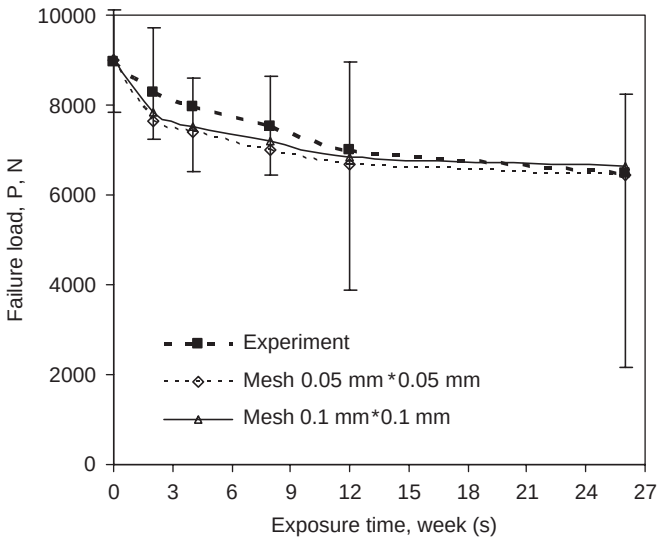

Fig. 10. Predicted ultimate failure load of the EA9321/aluminium SLJ using the continuum damage model.

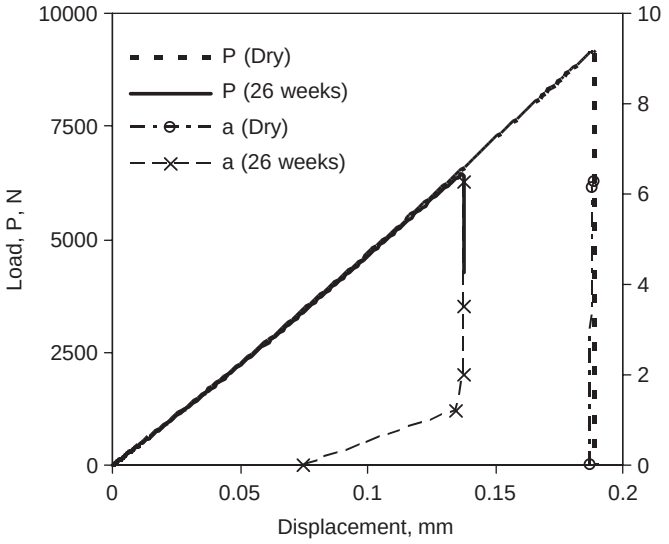

Fig. 12. Predicted loading history and damage propagation in an undegraded joint and a joint aged for 26 weeks (EA9321/aluminium SLJ, smallest mesh size 0.05 mm × 0.05 mm).

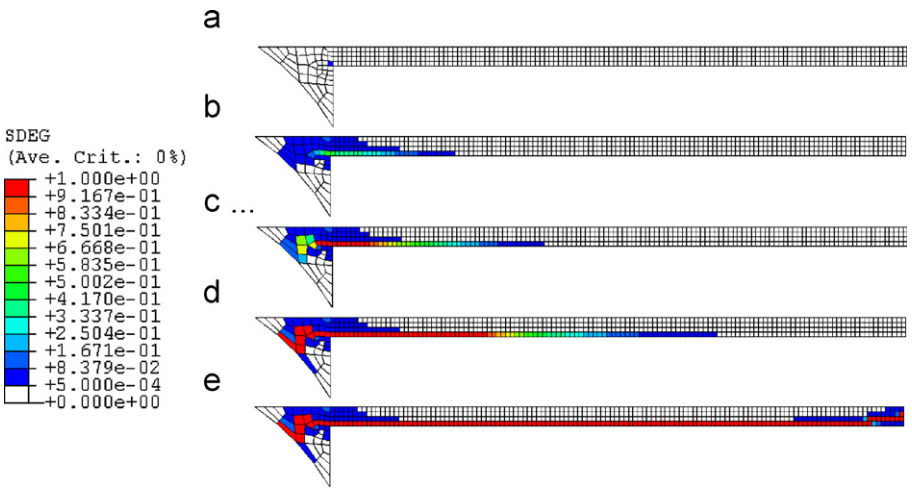

Fig. 11. Damage propagation in the EA9321/aluminium SLJ model (26 weeks degraded).

0.075 mm, and extended over 1.2 mm of the overlap as the applied displacement increased to 0.1345 mm. Failure then went though the rest of the adhesive layer with a very small additional increase in the applied displacement as the joint reached the ultimate load. It is worth noting that damage initiation in elements is different from failure of the elements. The elements only fail when the damage parameter reaches the maximum value of 1 as illustrated in Eq. (1). Damage initiation ($D>0$) was used in this plot, rather complete failure ($D=1$) as is the case using the strain-based failure model [6].

(b) *EA9321/composite SLJ model*: Progressive damage modelling of the EA9321/composite SLJ was also undertaken using the continuum damage model. Again, a half mesh model was created using four-noded plane strain quadrilateral elements with a mesh refinement of 0.05 mm × 0.05 mm. The mesh refinement was similar to that used for the aluminium SLJ shown in Fig. 9. The same moisture-dependent damage curves calibrated from the MMF analyses were used for the predictive modelling of this joint.

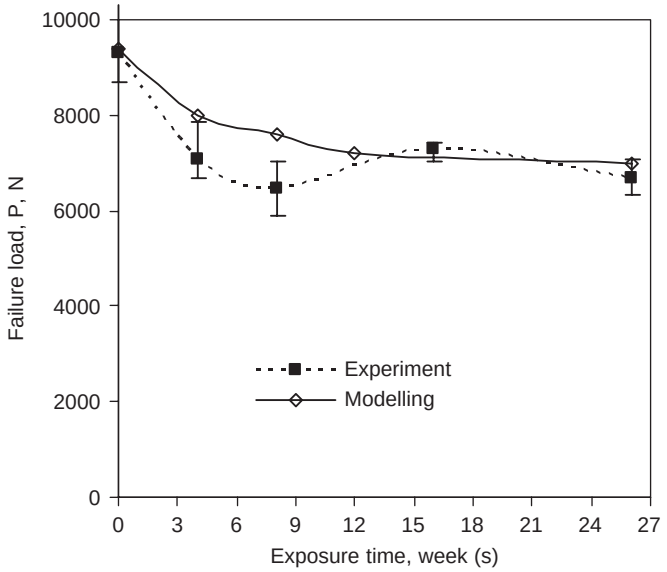

Fig. 13. Predicted ultimate failure load of the EA9321/composite SLJ using the continuum damage model (smallest mesh size 0.05 mm × 0.05 mm).

It is known that moisture can diffuse through the composite substrates of this joint as well as through the adhesive. The same standard Fickian diffusion model was used to specify the moisture diffusion for both the adhesive and the composite, using the parameters listed in Tables 1 and 3. The increase of moisture concentration in the adhesive with the substrates modelled as permeable was found significantly accelerated at extended exposure times [6]. As with the aluminium joints the moisture distribution was used as input for the coupled stress analysis phase. The predicted failure loads of the joint for the full range of exposure times are compared with the experimental results in Fig. 13. It can be seen that the predicted failure loads of the undegraded specimen matched the experimental results quite well and the degraded results showed a reasonable agreement at longer ageing times. However, the monotonic degradation trend in the predicted results does not match that of the experimental data. This may be due to the absence of the composite failure in the modelling, while delamination of the substrates did occur in the joints tested and might have caused the lower experimental failure load. Although only the modelled result with mesh scheme 0.05 mm × 0.05 mm is shown, the other mesh schemes (0.1 mm × 0.1 mm and 0.025 mm × 0.025 mm) have also been studied and the mesh independence of the continuum damage model was found as expected.

5. 3D progressive damage modelling

Modelling in 2D, as described in the previous section, may introduce limitations, both in the state of out of plane strain and stress and also by preventing moisture diffusion in the out of plane direction.

To ensure that the mesh independence of the moisture-dependent damage curves is still valid, a 3D MMF model with a uniform mesh refinement of 0.25 mm × 0.25 mm × 0.254 mm (shown in Fig. 14) was used for the predictive modelling using the 2D MMF calibration data first. The predicted results were very comparable to the 2D modelling results and the experimental data as shown in Fig. 15. The

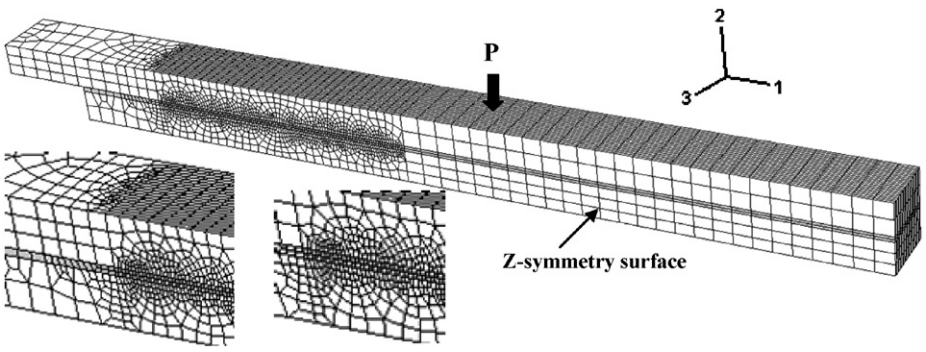

Fig. 14. 3D model of the MMF test and local mesh refinement used for the continuum damage model (smallest mesh size: 0.25 mm × 0.25 mm × 0.25 mm).

mesh independence of the continuum damage model has thus been further demonstrated.

A 3D model of the EA9321/aluminium SLJ was created (as a single part) with a cubic mesh refinement of 0.1 mm × 0.1 mm × 0.1 mm along the adhesive, due to the requirement for the elements to have an aspect ratio of unity when using the continuum damage model. However, this resulted in a massive model with more than 10^8 integration points to calculate. This was unsolvable on the hardware platform available. To avoid such a problem, an alternative method is to model and mesh the adhesive layer and the substrates separately, and then constrain or "tie" the contact surfaces together to make a contiguous model. It was found that the two constrained surfaces should have at least one side discretised with the same mesh density, as shown in the 1 direction of Fig. 16. A quarter model of the EA9321/aluminium joint with symmetry in the 3-direction and rotational symmetry was created. The mesh refinement along the adhesive layer was 0.1 mm × 0.1 mm × 0.1 mm and 0.1 mm × 1.0 mm × 1.0 mm in the two substrates adjacent to the adhesive, as shown in Fig. 16.

Although the same mesh density has been applied on both adhesive and substrates in the overlap length direction, the density in the other two directions were distinctly different. This may still result in a loss of accuracy because the integration points may not be properly interpolated. A stress analysis of this constrained model was thus undertaken and compared to an integrated 3D model with a coarse mesh before being used for the predictive modelling. It was found that the responses of the two models were consistent.

The predictive modelling was then applied to the 3D SLJ model. The largest 3D effect was likely to occur in the aluminium SLJ (where the lack of out of plane diffusion is not ameliorated by diffusing through the substrate [6]). Thus only the aluminium SLJ results have been presented in detail.

The same damage curves calibrated from the MMF tests were used for the adhesive. The predicted failure loads of the joint exposed for a range of times obtained from the 3D model are compared with the 2D modelling result and the experimental data in Fig. 17. It can be seen that the prediction of the 3D model agreed reasonably well with the experimental data and the 2D results. The largest difference between the 2D and 3D models occurs at the

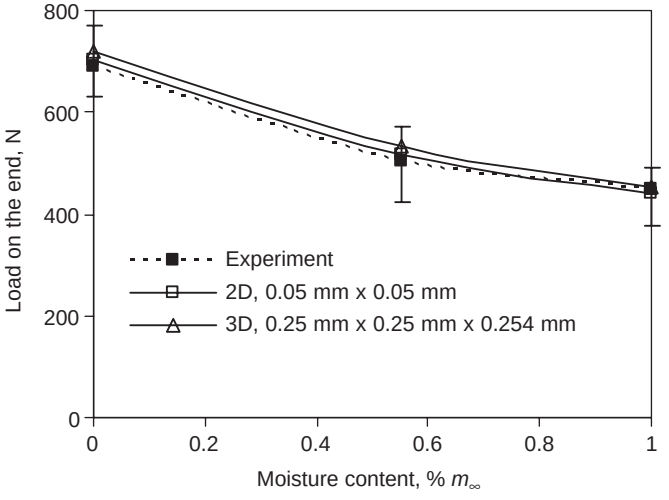

Fig. 15. Predicted failure loads from the 2D and 3D MMF models using the continuum damage model with the different mesh sizes.

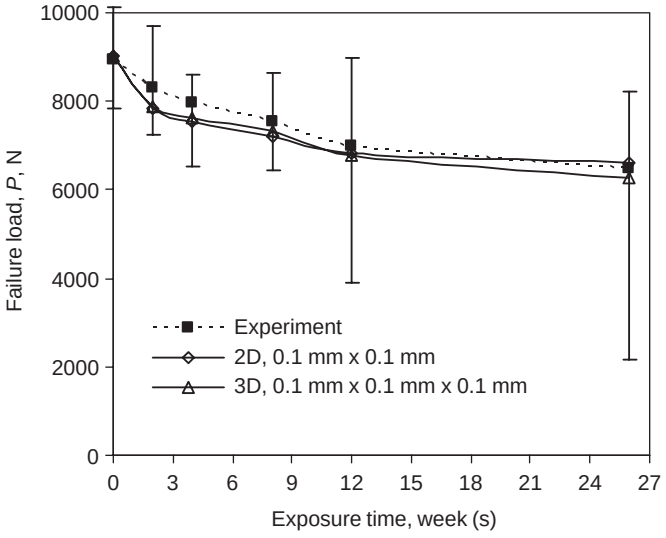

Fig. 17. Predicted ultimate failure load of the EA9321/aluminium SLJ using the continuum damage 2D and 3D models.

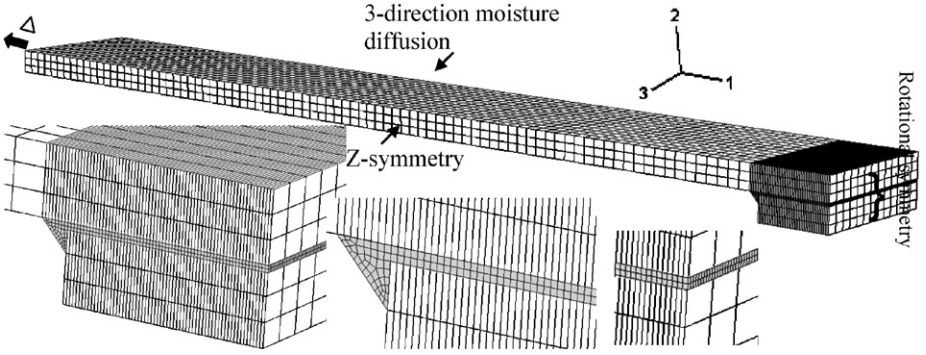

Fig. 16. 3D quarter symmetrical model of the EA9321/aluminium SLJ and local mesh refinement (smallest mesh size: 0.1 mm × 0.1 mm × 0.1 mm).

longest exposure time when the moisture transport in the out of plane direction is greatest.

The loading histories of the joint after being exposed for 26 weeks at 95.8% RH/50 °C, from both the 2D and 3D models, are compared in Fig. 18. It was found that the predicted failure load was reduced from the 2D to the 3D model by about 5% and the predicted stiffness was also reduced by a similar rate. This is consistent with the 3D prediction using the strain-based failure model [6]. The reduction in stiffness occurred because more of the adhesive-absorbed moisture and hence more of the adhesive had a reduced modulus, reducing the overall joint stiffness. Unlike the strain-based model, the continuum damage model defines damage initiation in the elements once D is greater than 0. The damage propagation was taken from the 1–2 plane of symmetry in the 3D model to correspond with the 2D (plane strain) model for the sake of comparison. It can be seen that the damage in the 3D model extended during the loading process, initially slowly along the overlap and then rapidly when the joint reached the ultimate load. This is consistent with the damage propagation plot obtained from the 2D model. This showed that the 2D (plane strain) model has been a reasonable simplification of the 3D model for this bonded joint.

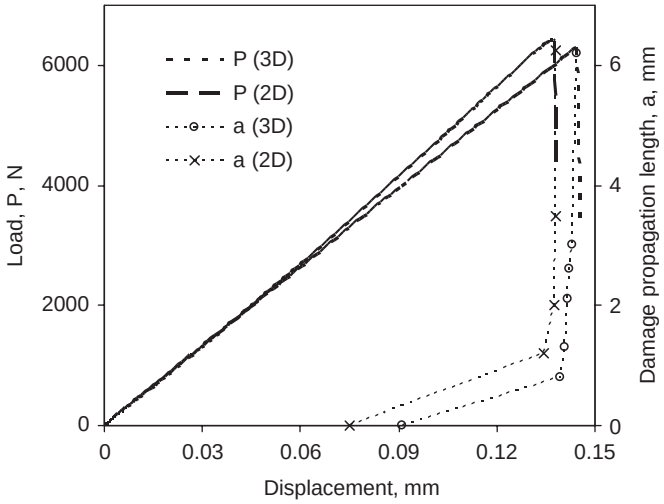

Fig. 18. Predicted loading history and damage propagation in a 3D and 2D EA9321/aluminium SLJ model after exposure for 26 weeks.

The spatial damage propagation in the 3D continuum damage model was also investigated and is illustrated using a series of contour plots in Fig. 19. The contours represent the damage parameter D. The arrows in Fig. 19 indicate the faces exposed to the environment. It can be observed in combination with Fig. 18 that the damage initiated around the corner of the joint at the saturated edge (A), rather than the less degraded mid-plane section (B), and then, propagated from the saturated corner to the middle (B) and the central section (C) of the adhesive layer relatively quickly. What is not clear from these figures is that failure also occurred in the lower layer of elements in the middle part of the joint. The edge of this is just visible around region (B) and first appears in Fig. 19(b). Final failure is illustrated in contour (d) after the load reached the ultimate resistance capacity of the joint. The critical failure path consists of fully damaged ($D = 1$) elements going through the saturated edge (A), similar to the 2D contour plot shown in Fig. 11. The fully damaged elements at the corner of the edge (C) give an indication of this failure path. This

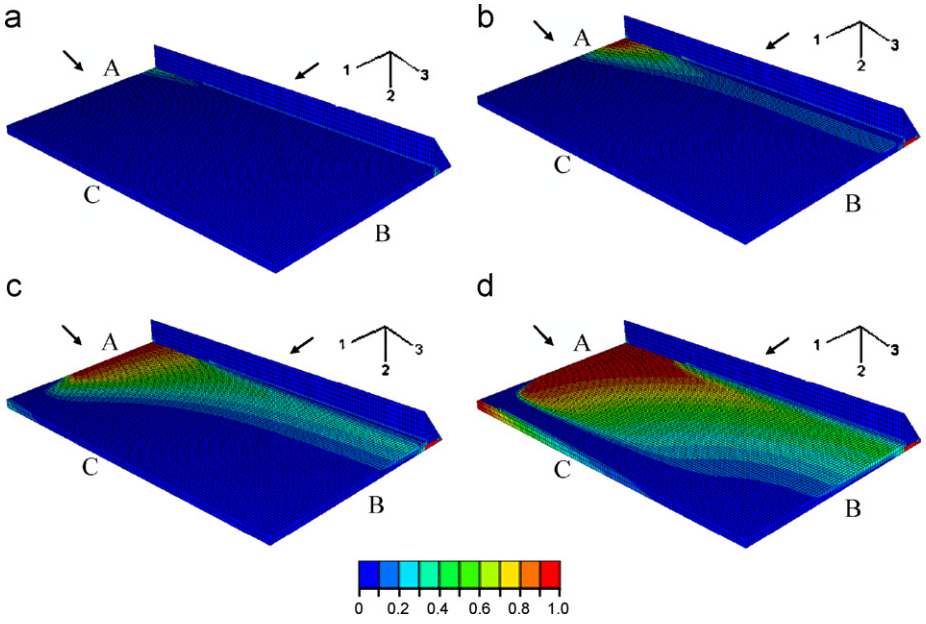

Fig. 19. 3D damage propagation in the EA9321/aluminium SLJ model using the continuum damage model (26 weeks degraded). At the applied displacement: (a) 0.0911 mm, (b) 0.1418 mm, (c) 0.1437 mm, (d) 0.1443 mm.

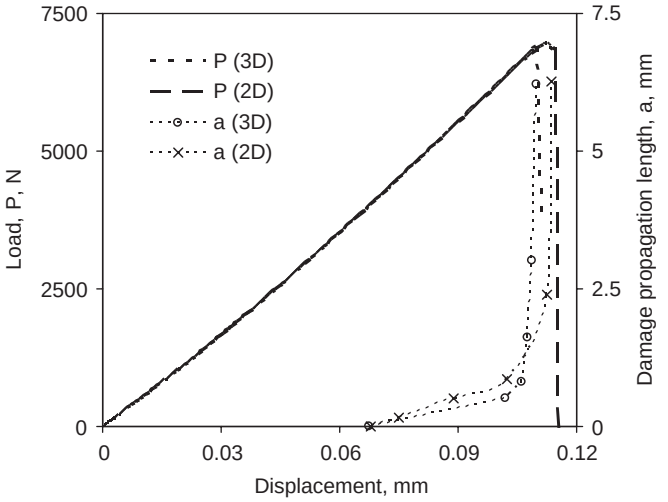

Fig. 20. Predicted loading history and damage propagation in a 3D and 2D EA9321/composite SLJ model after exposure for 26 weeks.

is not quite the same compared to the contour of the strain-based failure model [6]. This is probably due to the absence of the moderately damaged ($0<D<1$) elements because the strain-based failure model can only consider full damage ($D=1$) and thus cannot describe the real-damage propagation sufficiently.

Similar 3D analysis has been undertaken for the EA9321/composite SLJ and the same good predictions have been obtained using the scheme with diffusion through the substrates and the same moisture-dependent damage curves calibrated from the MMF tests. The predicted loading history of the joint, exposed for a 26-week period, is shown in Fig. 20. In this case, the predicted failure load and the joint stiffness for the 2D and 3D model were quite close. This can be explained as the orthotropic Young's modulus of the substrates is much higher (16 times) in the 1-direction than the other two directions as shown in Table 2. Thus adding the 3rd dimension did not significantly change the structural response of the joint. Furthermore, at the longer exposure times the moisture mainly diffused through the substrates and this was the same in both 2D and 3D models. The damage initiation and propagation in the adhesive of the EA9321/composite joint has not been shown because it was very similar to the EA9321/aluminium joint.

6. Conclusion

A continuum damage modelling method has been developed to model the progressive cohesive failure of the EA9321-bonded aluminium and composite single lap joints for a range of environmental degradation. The main advantage of this model is mesh independency, which derives from a damage parameter that is defined in terms of the equivalent plastic displacement, rather than strain.

A coupled diffusion-mechanical finite element analysis was implemented using the commercial software package ABAQUS. Both 2D and 3D modelling were considered. The predictions were very reasonable for a range of degradation when compared with the experimental results. The damage initiation and propagation during loading were also predicted correctly.

Compared with the strain-based failure model, the damage parameter incorporated in the continuum damage model can indicate not only the failure path but also the actual degree of the damage in the elements. This also results in a more gradual build up of damage in the joint which is more physically realistic.

Based on the encouraging results of the current study, predictive modelling of the environmental degradation in a series of butt joints bonded with another ductile adhesive (E32) is conducted, using the continuum damage model, and is described in a separate paper [28].

Acknowledgements

The authors would like to thank the Ministry of Defence for funding this work, David Liljedahl (University of Surrey) for experimental work on the EA9321 adhesive and the MMF specimens, Terry Ackerman (MBDA) for experimental work on the lap joints and Jeff Sargent (BAe Systems) for the composite diffusion measurements.

References

[1] Beevers A. Int J Mater Product Technol 1999;14:373–84.
[2] Loh WK, Crocombe AD, Abdel Wahab MM, Ashcroft IA. Eng Fract Mech 2002;69:2113–28.
[3] Loh WK, Crocombe AD, Abdel Wahab MM, Ashcroft IA. J Adhes 2003;79:1135–60.
[4] Liljedahl CDM, Crocombe AD, Wahab MA, Ashcroft IA. J Adhes Sci Tech 2005;19(7):525–47.
[5] Crocombe AD, Hua YX, Loh WK, Wahab MA, Ashcroft IA. Int J Adhes Adhes 2006;26:325–36.
[6] Hua Y, Crocombe AD, Wahab MA, Ashcroft IA. J Adhes 2006;82:135–60.
[7] Hua Y. Modelling environmental degradation in adhesively bonded joints. PhD thesis, University of Surrey, 2006.
[8] Gao H. J Mech Phys Solids 1996;44:1453–74.
[9] Zhang P, Klein P, Huang Y, Gao H, Wu PD. Comput Model Eng Sci 2002;3:263–78.
[10] Thiagarajan G, Hsia KJ, Huang YY. Eng Fract Mech 2004;71:401–23.
[11] Thiagarajan G, Huang YY, Hsia KJ. J Appl Mech (ASME Transactions) 2004;71:796–804.
[12] Lee EH. ASME J Appl Mech 1969;36:1–6.
[13] Gurson AL. J Eng Mater Technol 1977;99:2–15.
[14] Koplic J, Needleman A. Int J Solids Struct 1988;24:835–53.
[15] Chu CC, Needleman M. J Eng Mater Technol 1980;102:249–56.
[16] Needleman A, Tvergaard V. J Mech Phys Solids 1984;32:461–90.
[17] Needleman A, Tvergaard V. J Mech Phys Solids 1987;35:151–83.
[18] Reusch F, Svendsen B, Klingbeil D. Eur J Mech A/Solids 2003;22:779–92.
[19] Bonora N. J Strain Anal Eng Des 1999;34:463–78.
[20] Blocks W, Klingbeil D, Kunecke G, Sun DZ. ASTM STP 1244, Kirk, Bakker, editors., 1994.
[21] Lemaitre J. Eng Fract Mech 1986;25:523–37.

[22] Lemaitre J, Chaboche JM. Mechanics of Solid Materials. Cambridge: Cambridge University Press; 1985.
[23] Bonora N. Eng Fract Mech 1997;58:11–28.
[24] Crank J. The mathematics of diffusion. 2nd ed. Oxford Science Publications, 1975.
[25] ABAQUS /Explicit User's Manual, Version 6.5, Pawtucket: HKS Inc.; 2005.
[26] Turkmen HS, Loge RE, Dawson PR, Miller MP. Int J Fatigue 2003;25:267–81.
[27] Schon J, Nyman T, Blom A, Ansell H. Compos Sci Technol 2000;60:173–84.
[28] Hua Y, Crocombe AD, Wahab MA, Ashcroft IA. J Adhes Sci Technol 2007;21:179–95.